Available online at www.sciencedirect.com
SCIENCE DIRECT®
Fluid Phase Equilibria 235 (2005) 173–181
FLUID PHASE EQUILIBRIA
www.elsevier.com/locate/fluid

Liquid–solid equilibria under high pressure of tetradecane + pentadecane and tetradecane + hexadecane binary systems

M. Milhet [a,*], J. Pauly [a], J.A.P. Coutinho [b], M. Dirand [c], J.L. Daridon [a]

[a] *Laboratoire des Fluides Complexes, UMR 5150, B.P. 1155, 64013 Pau Cedex, France*
[b] *CICECO, Chemistry Department, Aveiro University, 3810-193 Aveiro, Portugal*
[c] *Laboratoire de Thermodynamique des Milieux Polyphasés, EA 3099, ENSIC, 54001 Nancy Cedex, France*

Received 25 March 2005; received in revised form 27 May 2005; accepted 6 June 2005

Abstract

The crystallization temperatures of two binary systems – tetradecane + hexadecane and tetradecane + pentadecane – were measured under high pressure up to 100 MPa using a polar microscopy device. The slopes of the melting curves in the (*T*, *P*) diagram show a dependence on the nature of the different solid phases that can appear. The effect of pressure on the liquidus curve in a (*T*, *x*) diagram is discussed and represented in the last part of this work with an excess Gibbs energy model, slightly modified to take the different solid phases into account.

Keywords: (Solid + liquid) equilibria; Binary system; *n*-Alkanes; Tetradecane; Pentadecane; Hexadecane; High pressure; Modelling

1. Introduction

Investigations into the phase behaviour of pure *n*-alkanes or waxy mixtures represent a major industrial and scientific concern. For example, the controlled precipitation of solid phases is widely applied in pharmaceutical, cosmetic and food industries as a separation process. In other areas like petroleum engineering, wax formation can be unwanted as it causes exploitation and transportation problems [1]. A response to these costly problems should be based on the development of adequate thermodynamic models, able to describe the phase behaviour of the very complex systems that crude oils are. This model development requires structural properties and accurate thermodynamic information about pure *n*-alkanes and synthetic mixtures. Most of the data available in the literature deal with the thermal behaviour of synthetic systems [2,3], degassed oils [4–7] and fuels [8,9] at atmospheric pressure. However, a good description of the influence of pressure on solid–liquid equilibria (SLE) has to be considered in most of the practical applications, leading recently to an increasing interest for experimental data under high pressure [10,11]. *n*-Alkane binary mixtures with eutectic points have to be carefully investigated, in particular the shift to higher temperatures of the liquidus curve due to an increase in pressure, the potential change of the eutectic composition and the structure of the different solid phases.

In this work, the crystallization temperatures of two binary mixtures, the tetradecane + hexadecane and tetradecane + pentadecane systems, have been measured by a cross polar microscopy device [12] that allows the study of phase equilibria up to 100 MPa. The results are compared with those obtained by a model previously proposed [13] in order to predict wax precipitation in complex mixtures under pressure.

2. Experimental

2.1. High-pressure microscope

In order to study the pressure influence on solid–liquid phase equilibria, a high-pressure microscope [12] was used to measure the crystallization temperatures of both binary systems. This experimental apparatus is built around an

* Corresponding author. Tel.: +33 5 59 40 76 92; fax: +33 5 59 40 76 95.
E-mail address: michel.milhet@univ-pau.fr (M. Milhet).

0378-3812/$ – see front matter © 2005 Elsevier B.V. All rights reserved.
doi:10.1016/j.fluid.2005.06.028

autoclave cell, made up of a stainless steel block and equipped with two sapphire windows through which the studied sample can be observed with the help of a polarizing microscope coupled with a video camera. This technique allows the detection of very small crystals, up to 2 μm in length, even when their concentration is too low for other approaches [14–18].

The temperature of the whole cell, between 243 and 373 K, is controlled by a heat-transducing fluid that circulates in flow lines designed in the metallic block. The thermal regulation of this fluid is carried out by a thermostat bath (HUBER) with a temperature stability of 0.01 K. The sample temperature is measured by means of a platinum resistance temperature detector (OMEGA) inserted inside a hole made in the cell. The uncertainty of temperature values is estimated at 0.2 K.

The pressure is transmitted to the sample through a hand pump and measured with a flush diaphragm pressure transmitter (DYNISCO), with a precision of 0.2%. This probe is regularly checked against a dead weight tester (BUDENBERG).

2.2. X-ray

X-ray diffraction was performed in a Philips X'Pert equipment which operates in the reflection mode with Cu Kα radiation (λ = 1.5406 Å). The temperature was controlled with a low-temperature Anton-Parr TTK450 chamber cooled by liquid nitrogen. Diffraction data were collected in a 2θ range from 4 to 75° with steps of 0.02 and a time per step of 2 s with incident and diffracted beam anti-scatter slits of 1°, divergence slit of 1°, receiving slit of 0.1 mm and curved graphite diffracted beam monochromator.

2.3. Experimental procedure

Due to important subcooling effects in paraffinic mixtures during crystallization, the phase change between the single liquid phase and the two-phase solid–liquid region is determined by measuring the disappearance conditions of the last crystals instead of the crystallization onset. As the studied mixtures are in liquid state at ambient temperature and atmospheric pressure, they are injected into the cell without any preliminary heating. Then, they are cooled in an isobaric process and maintained at about 2 K below the estimated solid disappearance temperature until equilibrium. After that, the samples are heated stepwise with an increase of 0.1–0.2 K every 5–10 min depending on the proximity of the cloud point, until disappearance of the last crystal.

2.4. Chemicals

The pure compounds used in this work were purchased from FLUKA, with purities better than 99 wt.% and were used without further purification. The binary mixtures were prepared by weighing, using high precision scales. The uncertainty of composition is within 0.01 mol.%.

3. Results and discussion

3.1. Study of tetradecane, pentadecane and hexadecane pure compounds

The melting temperatures of the three pure compounds at different pressures are reported with the results of binary systems in Table 1 for tetradecane (further noted n-C_{14}) and hexadecane (n-C_{16}), and in Table 2 for pentadecane (n-C_{15}). Deviations from literature data [19–26], listed in Table 3, show that our results are in good agreement with these data. The average deviation is 0.2 K for atmospheric measurements and 0.4 K for those carried out under pressure (the reference data have been interpolated with a polynomial function when the studied pressures were different).

3.2. Study of the tetradecane + hexadecane binary system

The liquidus temperatures at atmospheric pressure of the n-C_{14} + n-C_{16} binary system are listed in Table 1 and

Table 1
Liquidus temperatures in K of $\{(1-x)$ n-$C_{14} + x$ n-$C_{16}\}$ binary as a function of pressure for different compositions

x	0.1 MPa, T (K)	20 MPa, T (K)	40 MPa, T (K)	60 MPa, T (K)	80 MPa, T (K)	100 MPa, T (K)
0.000	279.2	284.2	289.1	293.8	297.9	301.7
0.050	278.1	282.9	287.5	291.8	296.3	300.4
0.100	277.5	282.2	286.7	291.2	295.4	299.5
0.150	276.7	281.5	285.8	290.1	294.1	298.5
0.175	276.2	280.3	284.4	288.2	291.9	295.6
0.200	276.5	280.7	284.7	288.5	292.3	295.9
0.250	277.0	281.3	285.4	289.3	292.9	296.5
0.400	279.5	284.2	288.1	292.0	295.8	299.3
0.500	283.2	288.0	292.0	296.7	300.9	305.1
0.600	285.1	289.8	294.1	299.1	303.7	307.4
0.750	288.3	293.0	297.4	301.8	306.3	310.6
0.830	288.9	293.6	298.2	302.9	307.2	311.4
0.900	290.3	295.1	299.6	304.1	308.4	312.7
1.000	291.5	296.0	300.4	304.8	309.7	313.5

Table 2
Liquidus temperatures in K of $\{(1-x)\ n\text{-}C_{14} + x\ n\text{-}C_{15}\}$ binary as a function of pressure for different compositions

x	0.1 MPa, T (K)	20 MPa, T (K)	40 MPa, T (K)	60 MPa, T (K)	80 MPa, T (K)	100 MPa, T (K)
0.000	279.2	284.2	289.1	293.8	297.9	301.7
0.050	278.1	282.8	287.4	291.9	296.3	300.4
0.100	277.4	282.1	286.7	291.2	295.5	299.7
0.100[a]	276.1[a]	280.4[a]	284.7[a]	288.7[a]	292.5[a]	296.3[a]
0.125	277.1	281.7	286.4	290.7	294.9	298.9
0.125[a]	276.3[a]	280.7[a]	284.9[a]	288.9[a]	292.8[a]	296.5[a]
0.150	276.2	280.6	284.8	288.8	292.7	296.3
0.200	276.7	280.9	285.1	289.1	292.9	296.7
0.250	276.9	281.2	285.3	289.4	293.2	296.9
0.500	278.7	283.0	287.3	291.3	295.1	298.8
0.750	280.8	285.2	289.5	293.5	297.4	301.1
1.000	283.2	287.8	291.9	296.2	300.1	303.9

[a] Melting temperature of the metastable rotator phase.

plotted in Fig. 1 where they are compared with literature data obtained by Metivaud et al. [27] and Rajabalee [28] using differential scanning calorimetry (DSC), and with those obtained by Parczewska [29] using both a kinetic [30] and a dilatometric [31] methods. These last results are in good agreement with ours. In the other hand, the comparison with Rajabalee's data seems to reveal a systematic shift between both series as his data are always lower than the values measured by microscopy. Visual microscopy is known to give higher crystallisation temperatures and more relevant values than other techniques for crude oils [14–17], which could explain a part of the difference observed. However, for some compositions, the deviation is greater than 2.5 K and remains too high in spite of the potential accumulation of all uncertainties. This may be explained by the appearance of a metastable phase and kinetic considerations.

Table 3
Deviations between experimental melting temperatures T_{exp} of pure n-C_{14}, n-C_{15} and n-C_{16} and literature data T_{ref} for different pressures

P (MPa)	$T_{exp} - T_{ref}$ (K)			
	n-C_{14}	n-C_{15}	n-C_{16}	
0.1	0.2^{19}	0.1^{20}		
0.1	0.1^{20}	0.0^{21}	0.2^{19}	
0.1	0.5^{21}	0.1^{22}	-0.1^{21}	
0.1	0.1^{22}	0.2^{24}	0.1^{22}	
0.1	0.5^{23}	0.6^{25}	0.3^{23}	0.3^{26}
20	0.1^{23}	0.4^{25}	-0.4^{23}	0.1^{26}
40	0.0^{23}	0.2^{25}	-0.9^{23}	-0.1^{26}
60	-0.1^{23}	0.3^{25}	-1.2^{23}	-0.2^{26}
80	-0.4^{23}	0.2^{25}	-0.6^{23}	0.2^{26}
100	-0.7^{23}	-0.2^{25}	-0.8^{23}	-0.3^{26}

In fact, when the liquid binary mixture crystallizes, it turns first into a translucent solid phase in most cases (Fig. 2), corresponding to a rotator phase R. Depending on the composition, this phase may or may not be stable. If the mole fraction of n-C_{16} is between the eutectic and the peritectic compositions, crystals are stable and remain in this state. But if the mixture composition is outside this range, the crystals are metastable and they end up by turning into an opaque triclinic phase Tp (Fig. 3), clearly different from the first phase.

The crystallographic study of Rajabalee [28] is in agreement with the different phases observed by microscopy, but his crystallization onsets measured by DSC seem to be underestimated for some compositions and should correspond to

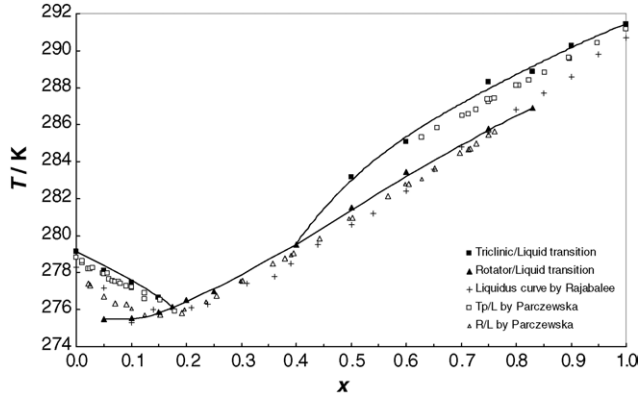

Fig. 1. Liquidus curve of the $\{(1-x)\ n\text{-}C_{14} + x\ n\text{-}C_{16}\}$ binary at atmospheric pressure.

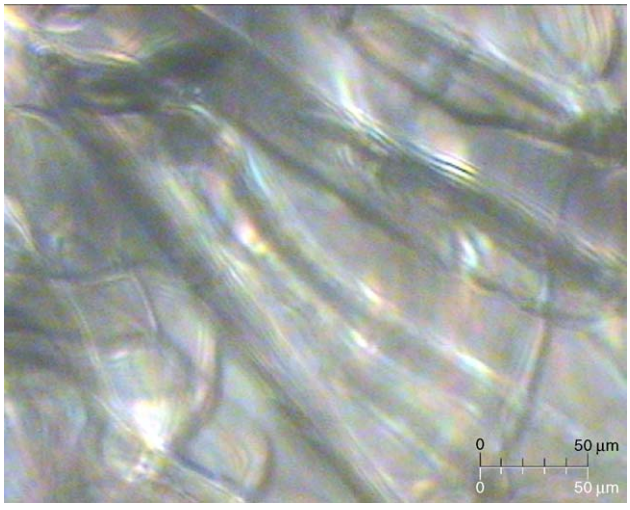

Fig. 2. Snapshot of rotator phase.

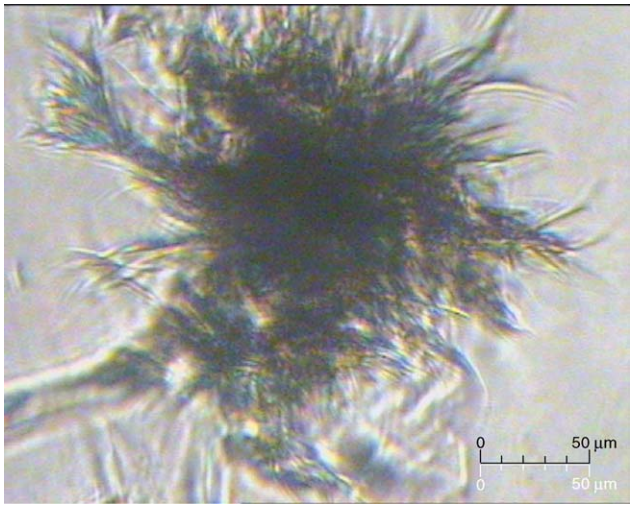

Fig. 3. Snapshot of triclinic phase.

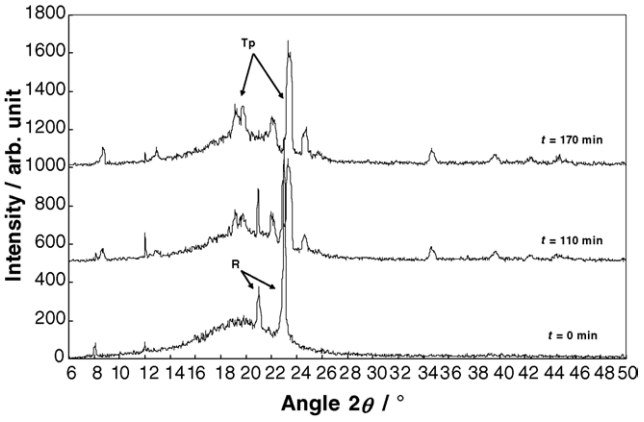

Fig. 4. X-Ray measurements: slow kinetics of transformation between the rotator metastable phase and the triclinic stable phase for the {0.17 *n*-C_{14} + 0.83 *n*-C_{16}} system.

the melting point of the metastable rotator phase. In fact, as can be seen in Fig. 4, the kinetics of transformation is very slow, and the triclinic stable phase can develop many hours after the rotator one and may be easily missed. In her work, Parczewska was not able to join the triclinic and the rotator melting lines in order to find the peritectic point due to the difficulty in making the triclinic phase appear for some compositions. The experimental device used in this work can considerably increase the rate by raising the pressure of the system for a short time, so that the phase change is almost instantaneous. Despite of the metastability of the rotator phase in these cases, it is possible to measure its melting temperature if a triclinic nucleus is not yet formed. The results are listed in Table 4 and plotted in Fig. 1 for comparison with the stable phases.

The high-pressure microscope allows liquid–solid equilibrium studies from atmospheric pressure up to 100 MPa. Measurements were performed in this range on the *n*-C_{14} + *n*-C_{16} binary system for each composition, every 20 MPa. As far as possible, the melting temperature of the metastable rotator phase was noted. But as the pressure increases, the triclinic nucleus appears more easily and the stable triclinic phase over-runs the whole sample, so that the disappearance temperature of the metastable phase can no longer be measured. The results are listed in Table 1 for the stable phase and in Table 4 for the metastable one. In both cases, the crystallization onset evolves quasi linearly with pressure. To quantify this pressure dependence, average slopes were calculated as follows:

$$\frac{\Delta T}{\Delta P} = \frac{T(P_{\max}) - T(P_0)}{P_{\max} - P_0} \quad (1)$$

For comparison purposes and in order to reduce the uncertainty of the calculated slopes, $P_{\max}$ was fixed at 100 MPa and P_0 corresponds to atmospheric pressure for all compositions. Thus, when the melting temperatures of the metastable phase are unavailable at 100 MPa, no slope value was given; in fact, as each curve is slightly bent, any slope calculation without this extreme point would be overestimated. The results are presented in Table 5. Plotting these slope values as a function of composition (Fig. 5) reveals that the average slope of the liquidus curves in the (T, P) diagram depends on the nature of the melting solid phase; the mean value of these slopes for the triclinic phase is equal to (0.222 ± 0.004) K MPa^{-1}, whereas it is equal to (0.196 ± 0.004) K MPa^{-1} for the rotator phase, whatever its stability.

Therefore, in addition to the visual difference between the rotator and triclinic phases, the study of pressure influence on crystallization temperatures can be used to characterize the melting solid phase.

Since the influence of pressure on crystallization temperature was studied for many compositions, it is interesting to see if pressure modifies the liquidus shape as well as eutectic

Table 4
Melting temperature in K of the metastable rotator phase as a function of pressure for the system {(1 − x) *n*-C_{14} + x *n*-C_{16}}

x	0.1 MPa, T (K)	20 MPa, T (K)	40 MPa, T (K)	60 MPa, T (K)	80 MPa, T (K)	100 MPa, T (K)
0.050	275.5	279.8	284.0	288.2	–	–
0.100	275.6	279.8	284.0	287.9	–	–
0.150	275.9	280.1	284.1	288.0	291.8	295.3
0.500	281.3	285.6	289.7	293.5	297.3	301.0
0.600	283.5	287.9	292.1	296.0	299.9	303.4
0.750	285.8	290.0	294.5	298.5	–	–
0.830	286.9	291.3	295.4	–	–	–

Table 5
Average slopes $\Delta T/\Delta P$ (K MPa^{-1}) of the liquidus curves in the (T, P) diagram calculated for each solid phase as a function of composition for $\{(1-x)$ n-$C_{14} + x$ n-$C_{16}\}$

x	Triclinic phase		Rotator phase	
0.000	0.225	±0.005		
0.050	0.223	±0.004		
0.100	0.221	±0.004		
0.150	0.218	±0.004	0.195	±0.004
0.175			0.195	±0.004
0.200			0.194	±0.004
0.250			0.195	±0.004
0.400			0.198	±0.004
0.500	0.220	±0.004	0.197	±0.004
0.600	0.223	±0.004	0.200	±0.004
0.750	0.223	±0.004		
0.830	0.225	±0.005		
0.900	0.224	±0.004		
1.000	0.220	±0.004		
Mean value	0.222	±0.004	0.196	±0.004

and peritectic points. For this purpose, the previous results from Table 1 have been plotted in Fig. 6.

It can be observed that all experimental isobaric liquidus plots present the same variations and shift monotonously to higher temperatures with increasing pressure. The eutectic and peritectic compositions are not displaced significantly with pressure as the calculated slopes for each solid phase are quite similar. Nevertheless, an increase in temperature difference between eutectic temperature and pure compound melting points with pressure can be observed, but it remains low, in the order of 3 K for an increase of 100 MPa.

3.3. Study of the tetradecane + pentadecane binary system

The same experiments were performed on the n-$C_{14} + n$-C_{15} system. The liquidus temperatures at atmospheric pressure are listed in Table 2 and plotted in Fig. 7, where they are compared with literature data [27,28,32]. As for the previous system, a systematic shift is observed between both series, and goes increasing when the composition of the binary mixture approaches the eutectic composition. The important deviations observed correspond to the formation of a metastable rotator phase.

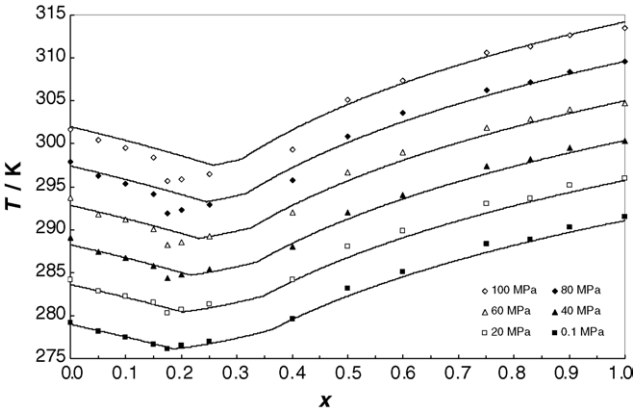

Fig. 6. Experimental liquidus points for the $\{(1-x)\,n$-$C_{14} + x\,n$-$C_{16}\}$ system for six pressures in the range 0.1–100 MPa (solid line: modelling results).

The pressure influence on crystallization temperatures was also studied. Plotting the results of Table 2 for a given composition once again reveals a quasi-linear relationship between pressure and temperature. Average slopes were calculated (Table 6) and plotted as a function of composition in Fig. 8. As for the previous binary system, the average slope of the liquidus curves in the (T, P) diagram depends on the nature of the melting solid phase. The mean value of these slopes for the triclinic phase is equal to (0.223 ± 0.004) K MPa^{-1}, whereas it is equal to (0.202 ± 0.004) K MPa^{-1} for the rotator phase. These slopes are similar to those of the n-$C_{14} + n$-C_{16} system and confirm that the pressure influence on crystallisation temperatures can be used to characterize the melting solid phase.

The pressure influence on the liquidus curve was studied by plotting the results of Table 2 in Fig. 9. As for the previous study, the different isobars have the same shape and

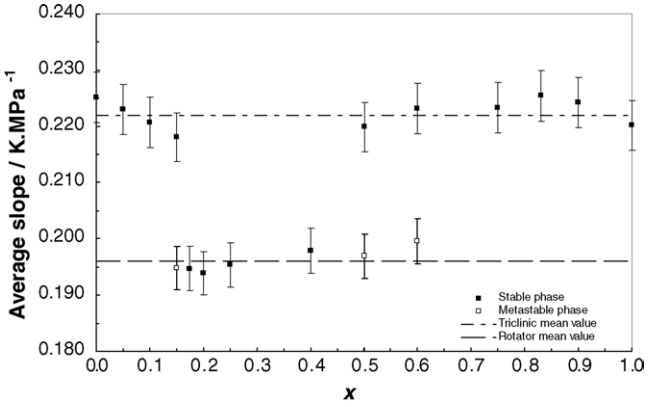

Fig. 5. Average slopes $\Delta T/\Delta P$ of the liquidus curves in the (T, P) diagram calculated for each solid phase as a function of composition for $\{(1-x)$ n-$C_{14} + x$ n-$C_{16}\}$.

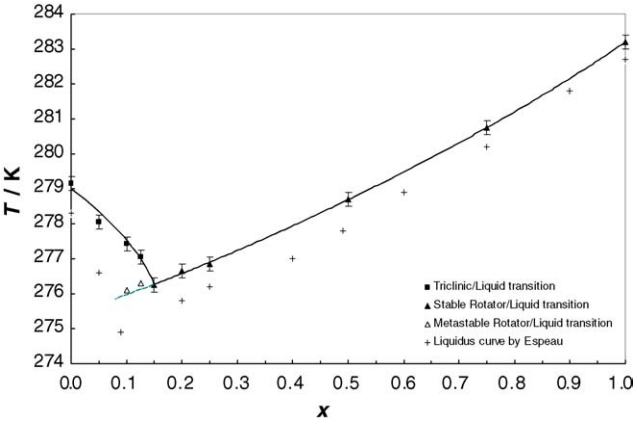

Fig. 7. Liquidus curve of the $\{(1-x)\,n$-$C_{14} + x\,n$-$C_{15}\}$ binary at atmospheric pressure.

Table 6
Average slopes $\Delta T/\Delta P$ (K MPa^{-1}) of the liquidus curves in the (T, P) diagram calculated for each solid phase as a function of composition for $\{(1-x)$ n-$C_{14}+x$ n-$C_{15}\}$

x	Triclinic phase		Rotator phase	
0.000	0.225	±0.005		
0.050	0.224	±0.004		
0.100	0.223	±0.004	0.202	±0.004
0.125	0.218	±0.004	0.202	±0.004
0.150			0.201	±0.004
0.200			0.201	±0.004
0.250			0.200	±0.004
0.500			0.201	±0.004
0.750			0.204	±0.004
1.000			0.208	±0.004
Mean value	0.223	±0.004	0.202	±0.004

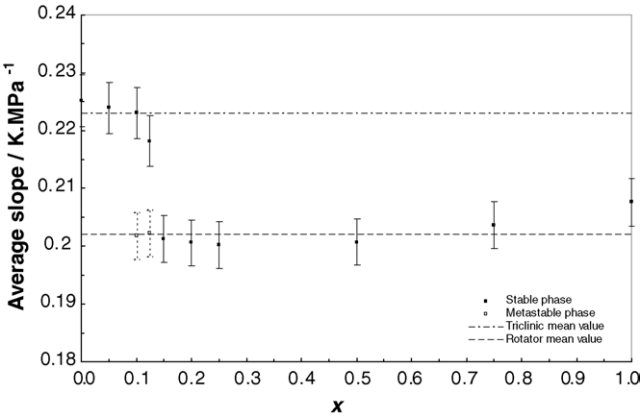

Fig. 8. Average slopes $\Delta T/\Delta P$ of the liquidus curves in the (T, P) diagram calculated for each solid phase as a function of composition for $\{(1-x)$ n-$C_{14}+x$ n-$C_{15}\}$.

shift monotonously to higher temperature with increasing pressure. Although the eutectic point is more visible when pressure increases, its composition does not vary significantly.

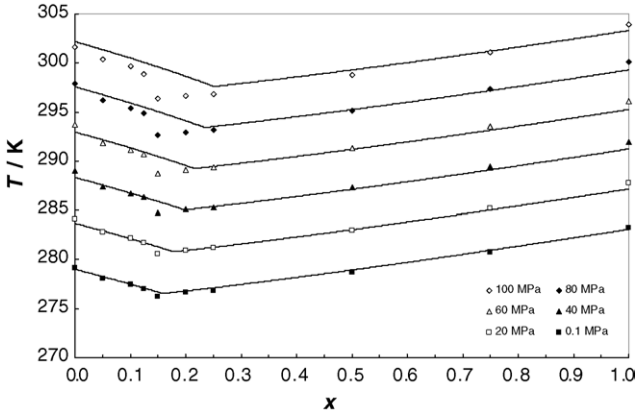

Fig. 9. Experimental liquidus points for the $\{(1-x)$ n-$C_{14}+x$ n-$C_{15}\}$ system for six pressures in the range 0.1–100 MPa (solid line: modelling results).

3.4. Modelling

Equilibrium conditions are obtained from the equality of fugacities of each component in both liquid and solid phases:

$$f_i^{\mathrm{L}}(T, P, x_i^{\mathrm{L}}) = f_i^{\mathrm{S}}(T, P, x_i^{\mathrm{S}}) \tag{2}$$

The liquid phase fugacities can be written as:

$$f_i^{\mathrm{L}}(T, P, x_i^{\mathrm{L}}) = P x_i^{\mathrm{L}} \phi_i^{\mathrm{L}} \tag{3}$$

where the fugacity coefficient ϕ_i^{L} is calculated using the Peng–Robinson equation of state [33], with the pure compound coefficients obtained from the correlations proposed by Robinson et al. [34]. Mixing rules are classical, i.e. quadratic for a and linear for b, and the interaction parameter k_{ij} is set to zero. The volumetric properties calculated by the Peng–Robinson EOS are corrected using the volume translation proposed by Peneloux et al. [35].

The solid phase fugacities at a pressure P are obtained by the equation:

$$\ln\, f_i^{\mathrm{S}}(P) = \ln\, f_i^{\mathrm{S}}(P_0) + \frac{1}{RT}\int_{P_0}^{P} \overline{V}_i^{\mathrm{S}}\, \mathrm{d}P \tag{4}$$

where the fugacity of the component i in the solid phase at pressure P_0 is calculated from its fugacity in subcooled liquid state at the same temperature T:

$$f_i^{\mathrm{S}}(P_0) = x_i^{\mathrm{S}} \gamma_i^{\mathrm{S}}(P_0) f_i^{0,\mathrm{L}}(P_0)\, \exp\left[-\frac{\Delta_{\mathrm{fus}} H_i}{RT}\left(1-\frac{T}{T_{\mathrm{fus},i}}\right)\right] \tag{5}$$

where γ_i^{S} represents the activity coefficient of the compound i in the solid phase; $T_{\mathrm{fus},i}$ and $\Delta_{\mathrm{fus}}H_i$ are, respectively, the fusion temperature and the enthalpy of fusion of the pure compound i. The Poynting correction term of Eq. (4) is simplified by the assumption that the partial molar volume of each component is proportional to the subcooled liquid molar volume:

$$\overline{V}_i^{\mathrm{S}} = V_i^{0,\mathrm{S}} = \beta V_i^{0,\mathrm{L}} \tag{6}$$

where β is assumed to be pressure independent, so that Eq. (4) can be written as proposed by Pauly et al. [13,36–40]:

$$f_i^{\mathrm{S}}(T, P, x_i^{\mathrm{S}}) = x_i^{\mathrm{S}} \gamma_i^{\mathrm{S}} \left[f_i^{0,\mathrm{L}}(T, P_0)\right]^{1-\beta} \left[f_i^{0,\mathrm{L}}(T, P)\right]^{\beta} \times \exp\left[-\frac{\Delta_{\mathrm{fus}} H_i}{RT}\left(1-\frac{T}{T_{\mathrm{fus},i}}\right)\right] \tag{7}$$

In this work, as shown in the first part of this paper, the solid phases that can appear during crystallization are either rotator or triclinic. While working with rotator phases, one must remember that this kind of crystalline structure does not exist for pure even alkanes lighter than eicosane. Now, modelling of phase equilibria requires considering each component in the same state for the calculation of fugacities. For this purpose, we have interpolated the data for the odd

alkanes published by Broadhurst et al. [41] to obtain the melting temperatures and the enthalpies of fusion of tetradecane and hexadecane in a hypothetical rotator state. This is possible because the crystallization temperatures of these rotator phases are always below the real melting point of the pure even compound, so the stability of the different phases is not altered.

The coefficient β in Eq. (7) is intimately linked to the pressure effect on crystallization temperatures. As the average slope calculated with Eq. (1) for the triclinic solid phase is greater than for the rotator phase, the value of the coefficient β will be different for each phase. The best results (Figs. 6 and 9) were obtained with the value $\beta^{R} = (0.908 \pm 0.002)$ for the rotator phase, and $\beta^{T} = (0.852 \pm 0.003)$ for the triclinic one. A review of the data published by Nelson et al. [42], Templin [43], Shaerer et al. [44], Van Hook et al. [45] and Würflinger et al. [46,47] on the volume change during crystallization of pure *n*-alkanes between *n*-C_9 and *n*-C_{26} was used to calculate average values of the beta coefficient in Eq. (6) for each kind of transformation, i.e. $\beta^{R} = (0.90 \pm 0.01)$ for a rotator melting phase and $\beta^{T} = (0.85 \pm 0.01)$ for a triclinic phase. These results are in agreement with our fitted values and confirm that excess volumes are negligible for mixtures of nearly similar alkanes.

The activity coefficients γ_i^{S} of the rotator phase were described by means of the Chain Delta Lattice Parameter (CDLP) model, developed by Coutinho et al. [48], where the excess Gibbs energy is given by:

$$g^{E} = \theta \frac{(l_l - l_s)^2}{{l_s}^3} x_l x_s \tag{8}$$

where l_l is the length of crystalline cell of the longest molecule, l_s the length of the shortest molecule and $\theta = 2317$ kJ Å mol^{-1}, a parameter given by the authors. Used as it is, the CDLP model gives good predictive results, as the average absolute deviations (AAD) are 0.3 and 0.4 K, respectively, for the *n*-C_{14} + *n*-C_{15} and the *n*-C_{14} + *n*-C_{16} systems.

Despite these good results, the Wilson equation [49] was also tested in the hope of decreasing the AADs, though it was initially proposed for the orthorhombic solid phase. The excess Gibbs energy is calculated with:

$$\frac{g^{E}}{RT} = -x_l \ln \left[x_l + x_s \exp\left(-\frac{\lambda_{ls} - \lambda_{ll}}{RT} \right) \right] - x_s \ln \left[x_s + x_l \exp\left(-\frac{\lambda_{ls} - \lambda_{ss}}{RT} \right) \right] \tag{9}$$

where the interaction energies λ_{ll}, λ_{ss} and $\lambda_{ls} = \lambda_{ss}$ are obtained from:

$$\lambda_{ii} = -\frac{2}{Z_{axial}} (\Delta_{sub} H - RT) \tag{10}$$

with $Z_{axial} = 6$ according to Coutinho et al. [48].

The original model works perfectly with the *n*-C_{14} + *n*-C_{16} system (AAD = 0.2 K), but it was necessary to correct the interaction energy $\lambda_{ls} = \lambda_{ss}(1 + \alpha_{ls})$ between *n*-C_{14} and *n*-C_{15} molecules using the α_{ls} parameter proposed by Coutinho et al. [48]. The correlation the authors introduced is not suitable for this case, as it was developed for alkanes of higher molecular weight, above *n*-C_{20}. Here, a value of $\alpha_{ls} = -0.017$ gives results that match experimental data, with an AAD of 0.3 K. For the binary systems studied in this work, both the CDLP model and the Wilson equation lead to equivalent accuracies, but the CDLP model will be preferred because of its predictive character.

The triclinic phase was modelled using a Margules g^{E} model with one parameter:

$$g^{E} = \Omega x_l x_s \tag{11}$$

Average absolute deviations of 0.2 and 0.4 K were calculated for the *n*-C_{14} + *n*-C_{16} and for the *n*-C_{14} + *n*-C_{15} system, respectively. Despite these low deviations, the predicted liquidus curves lead to an overestimation of the eutectic composition and, where appropriate, to an underestimation of the peritectic composition. These tendencies cannot be improved even if a higher value of Ω is chosen to increase the non-ideality of the triclinic phase or if a two coefficient model is used, as the liquidus lines seem to have reached their maximal curvature.

4. Conclusion

The liquid–solid equilibria under pressure (up to 100 MPa) of the tetradecane + pentadecane and tetradecane + hexadecane binary systems were studied with a high pressure microscopy device as described in the first part of this paper. As this technique allows visual monitoring of the samples, it is possible to distinguish the different crystalline structures – rotator or triclinic – that appear in solid phases, and to measure their melting point, even for metastable phases. Plotting these crystallization temperatures versus pressure shows that the slopes of the straight lines obtained are characteristic of the nature of the melting crystal, whatever its stability. In a (T, x) diagram, liquidus curves are regularly shifted towards higher temperatures with an increase in pressure, but the compositions of the eutectic and peritectic points are not significantly displaced in the range 0.1–100 MPa.

In order to model the behaviour of these binary systems, the Peng–Robinson equation of state was used for the liquid phase, whereas excess Gibbs energy models were chosen for solid phases. The Chain Delta Lattice Parameter model leads to predictive results in very good agreement with experimental data for the stable and the metastable rotator phases, with an average absolute deviation less than 0.4 K. The strong non-ideality of the triclinic phases was rendered thanks to a Margules type equation but the description of the liquidus curves in these cases is not accurate enough to predict properly the melting temperatures and the compositions of eutectic and peritectic points when pressure increases. New values

of the beta coefficient introduced by Pauly et al. [13] were given in order to take the crystalline structure into account for rendering pressure influence on solid–liquid equilibria, i.e. $\beta^{R} = (0.908 \pm 0.002)$ and $\beta^{T} = (0.852 \pm 0.003)$, respectively, for the rotator phase and for the triclinic one.

List of symbols

a, b	EOS parameters
g^{E}	excess Gibbs energy
$\Delta_{fus} H$	molar enthalpy of fusion of pure compound
k	binary interaction parameter
l	molecule length
P	pressure
P_{max}	maximal pressure
P_0	atmospheric pressure
R	gas constant, or symbol of rotator phase
T	temperature
Tp	symbol of triclinic phase
T_{fus}	melting temperature of pure compound
V	molar volume
$\overline{V}$	partial molar volume
x	molar fraction
Z_{axial}	coordination number

Greek letters

α	correction of interaction energy
β	coefficient introduced in Eq. (6)
Δ	change of values
ϕ	fugacity coefficient
γ	activity coefficient
λ	wavelength of the radiation used for diffraction, or binary interaction energy
θ	angle of diffraction, or parameter in Eq. (8)
Ω	parameter of Margules model

Superscripts

0	pure compound
L	liquid phase
R	rotator phase
S	solid phase
T	triclinic phase

Subscripts

i	compound number i
l	long molecule
s	short molecule

Acknowledgements

Sincere thanks to Pr. R.A. Heidemann and Pr. M. Parsons for their valuable help. Financial support from FEDER and FCT (Project POCTI/CTM/60288/2004) is gratefully acknowledged by J.A.P. Coutinho.

References

[1] S. Misra, S. Baruah, K. Singh, SPE Prod. Facilities 10 (1995) 50–54.
[2] J.A.P. Coutinho, S.I. Andersen, E.H. Stenby, Fluid Phase Equilib. 103 (1995) 23–39.
[3] J.A.P. Coutinho, K. Knudsen, S.I. Andersen, E.H. Stenby, Chem. Eng. Sci. 51 (1996) 3273–3282.
[4] K.W. Won, Fluid Phase Equilib. 30 (1986) 265–279.
[5] J.H. Hansen, A. Fredenslund, K.S. Pedersen, H.P. Rønningsen, AIChE J. 34 (1988) 1937.
[6] K.S. Pedersen, P. Skovborg, H.P. Rønningsen, Energy Fuels 5 (1991) 924–932.
[7] C. Lira-Galena, A. Firoozabadi, J.M. Prausnitz, AIChE J. 42 (1996) 239–248.
[8] J.A.P. Coutinho, V. Ruffier-Meray, Ind. Eng. Chem. Res. 36 (1997) 4977–4983.
[9] J.A.P. Coutinho, Energy Fuels 14 (2003) 625–631.
[10] P. Morawski, J.A.P. Coutinho, U. Domańska, Fluid Phase Equilib. 230 (2005) 72–80.
[11] U. Domańska, P. Morawski, Fluid Phase Equilib. 218 (2004) 57–68.
[12] J.-L. Daridon, J. Pauly, M. Milhet, Phys. Chem. Chem. Phys. 4 (2002) 4458–4461.
[13] J. Pauly, J.-L. Daridon, J.A.P. Coutinho, N. Lindeloff, S.I. Andersen, Fluid Phase Equilib. 167 (2000) 145–159.
[14] T.G. Monger-McClure, SPE Prod. Facilities 14 (1999) 4–16.
[15] H.-Y. Ji, B. Tohidi, A. Danesh, A.C. Todd, Fluid Phase Equilib. 216 (2004) 201–217.
[16] H.P. Rønningsen, B. Bjorndal, A.B. Hansen, W.B. Pedersen, Energy Fuels 5 (1991) 895–908.
[17] A. Hammami, M. Raines, SPE 38776 (1997) 273–287.
[18] V.R. Kruka, E.R. Cadena, T.E. Long, J. Pet. Technol. 47 (1995) 681–687.
[19] R.L. Snow, J.B. Ott, J.R. Goates, K.N. Marsh, S. O'Shea, R.H. Stokes, J. Chem. Thermodynamics 2 (1986) 107–130.
[20] J.F. Messerly, G.B. Guthrie, S.S. Todd, H.L. Finke, J. Chem. Eng. Data 12 (1967) 338–346.
[21] W.F. Seyer, R.F. Patterson, J.L. Keays, J. Am. Chem. Soc. 66 (1944) 179–182.
[22] H.L. Finke, M.E. Gross, G. Waddington, H.M. Huffman, J. Am. Chem. Soc. 76 (1954) 333–341.
[23] Y. Tanaka, M. Kawakami, Fluid Phase Equilib. 125 (1996) 103–114.
[24] R.R. Nelson, W. Webb, J.A. Dixon, J. Chem. Phys. 33 (1960) 1756–1764.
[25] A. Würflinger, G.M. Schneider, Ber. Bunsen-Ges. Phys. Chem. 77 (1973) 121–128.
[26] A. Würflinger, M. Sandmann, Z. Naturforsch. 55a (2000) 533.
[27] V. Metivaud, F. Rajabalee, H.A.J. Oonk, D. Mondieig, Y. Haget, Can. J. Chem. 77 (1999) 332–339.
[28] F. Rajabalee, European Thesis of the University Bordeaux I, France, 1995 pp. 170–178.
[29] B. Parczewska, Thesis of the Institute of Physical Chemistry, Polish Academy of Sciences, Poland, 1998 pp. 86–92.
[30] Z. Plesnar, P. Gierycz, A. Bylicki, Thermochim. Acta 128 (1988) 93–98.
[31] B. Parczewska, J. Chem. Thermodynamics 32 (2000) 777–788.
[32] P. Espeau, European Thesis of the University Bordeaux I, France, 1995 pp. 113–118.
[33] D.Y. Peng, D.B. Robinson, Ind. Eng. Chem. Fundam. 15 (1976) 59–64.
[34] D.B. Robinson, D.Y. Peng, GPA Research Report 28, Tulsa, 1978.
[35] A. Peneloux, E. Rauzy, R. Frèze, Fluid Phase Equilib. 8 (1982) 7.C.H.
[36] J. Pauly, J.-L. Daridon, J.A.P. Coutinho, Fluid Phase Equilib. 187 (2001) 71–82.
[37] J. Pauly, J.-L. Daridon, J.A.P. Coutinho, F. Montel, Energy Fuel 15 (2001) 730–735.

[38] J. Pauly, J.-L. Daridon, J.M. Sansot, J.A.P. Coutinho, Fuel 82 (2003) 595–601.
[39] J.M. Sansot, J. Pauly, J.-L. Daridon, J.A.P. Coutinho, AICHE J. 51 (2005) 7.
[40] J. Pauly, J.-L. Daridon, J.A.P. Coutinho, M. Dirand, Fuel 84 (2005) 453–459.
[41] M.G. Broadhurst, J. Res. Nat. Bur. Stand. 6A (1962) 241–249.
[42] R.R. Nelson, W. Webb, J.A. Dixon, J. Chem. Phys. 33 (1960) 1756–1764.
[43] P.R. Templin, Ind. Eng. Chem. 48 (1956) 154.
[44] A.A. Schaerer, C.J. Busso, A.E. Smith, L.B. Skinner, J. Am. Chem. Soc. 77 (1955) 2017–2018.
[45] A. van Hook, L. Silver, J. Chem. Phys. 10 (1942) 686.
[46] A. Würflinger, G.M. Schneider, Ber. Bun. Ges. Phys. Chem. 77 (1973) 121–128.
[47] A. Würflinger, Colloid Polym. Sci. 262 (1984) 115–118.
[48] J.A.P. Coutinho, K. Knudsen, S.I. Andersen, E.H. Stenby, Chem. Eng. Sci. 51 (1996) 3273–3282.
[49] G.M. Wilson, J. Am. Chem. Soc. 86 (1964) 127–130.